2017 IEEE International Conference on Advanced Intelligent Mechatronics (AIM)
Sheraton Arabella Park Hotel, Munich, Germany, July 3-7, 2017

Parametric Design and Analysis of a New 3D Compliant Manipulator for Micromanipulation

Abdullah T. Elgammal [a], Mohamed Fanni [b], Manar Lashin [c], Mahmoud Magdy [d], Abdelfatah M. Mohamed [e]

***Abstract*— This paper introduces a parametric design of a new 3D compliant parallel manipulator based on pantograph linkage for micro/nano applications. Furthermore, the modal shapes and natural frequencies analysis are carried out versus the flexure joint parameters which are a crucial point for the controller selection/design and geometry optimization. The new compliant manipulator provides decoupled 3DOF translational motion with fixed orientation of the end effector and it has significantly high workspace to size ratio. The modified manipulator aims to enlarge the workspace by enhancing the values of magnification factors of input motion and by reducing the parasitic motion and geometric stiffening of the original manipulator. The main parameters that affect the performance of the compliant manipulator are determined based on the generated results of finite element analysis which is performed using ANSYS software. The results have successfully demonstrated the improvements of the proposed manipulator in terms of workspace size, magnification factors, joint stiffening and parasitic motions.**

I. INTRODUCTION

Micromanipulators are required to manipulate minute objects for performing tasks such as bio-cell manipulation, scanning tunneling microscope (STM), atomic force microscope (AFM), and micro-assembly. These tasks demand high precision and dexterity which enable an unprecedented level of manipulability [1]. Compliant mechanisms have monolithic structures that provide the required motion from deflections by way of flexure hinges and/or flexible links inherent to the structure. Instead of traditional rigid-body mechanism, compliant mechanism endows several merits including no backlash, free of friction and lubrication, vacuum compatibility, low cost and easy to fabricate [2]. Additionally, it can overcome the shortcomings existing in conventional precision systems with sliding and rolling bearings, and implement positioning with the capability of smooth motion [3]. Flexure hinge-based compliant parallel manipulators can be utilized for micro-positioning applications in which high precision actuators are required [4]. A major drawback with compliant based parallel manipulators is the coupled motions that increase the complexity of the kinematic, dynamic analysis and control [5]. The decoupled motion implies that each actuator delivers motion in one independent direction only. In [6] a novel design of 3D compliant manipulator in a simple and compact structure for micromanipulation is introduced. The workspace volume to size ratio of this new manipulator is higher than those of beforehand reported designs. The parametric design of compliant mechanisms is relatively new and considered as one of the main difficulties associated with it. Contrary to the design methods of rigid-body mechanisms that have seen a great progress in their techniques [7].

Parametric design needs to predict the force and deflection of the compliant mechanism which is difficult because it undergoes a highly nonlinear behavior and it is experience-based. Over the past years, studies have provided the impact of frequency analysis on compliant parallel manipulators (CPM) [8]. Study of natural frequencies is a critical point for controller selection and in the selection of optimal design dimensions as the frequencies show the way a mechanism tends to vibrate. The highest level of energy due to vibration can be inferred from the first natural frequency [9]. The common methods of modeling of the compliant mechanisms are the elliptic integral solution, pseudo-rigid-body model (PRBM) and Finite Element Analysis (FEA). The elliptic integral solution is frequently thought to be the most precise and complex method [10], while PRBM is used to simplify the analysis and design of compliant mechanisms [11]. Finite element method is a time-consuming method which provides fine tune for the design and it is widely used for analysis [12].

The aim of this paper is to introduce a parametric design of the 3DOF compliant manipulator In [6] with a circular notch joint. Modal analysis is carried out with the mode shapes and natural frequencies. This study will assist in a reasonable selection of the control strategy and provides a useful information for optimal geometry design. This paper is organized as follows. The description and kinematic modeling of the new CPM are presented in Section II. Parametric Design is proposed in Section III. Modal analysis and simulation using ANSYS are explained in Section IV. Finally, conclusions are drawn in Section V.

[a]Mechatronics and Robotics Eng. Dept., Egypt-Japan University of Science and Technology, E-JUST- Alexandria, Egypt abdallah.gammal@ejust.edu.eg
[b]Mechatronics and Robotics Eng. Dept., Egypt-Japan University of Science and Technology, E-JUST- Alexandria, Egypt, on leave: Production Engineering and Mechanical Design Department, Faculty of Engineering, Mansoura University, Egypt mohamed.fanni@ejust.edu.eg
[c]Mechatronics and Robotics Eng. Dept., Egypt-Japan University of Science and Technology, E-JUST- Alexandria, Egypt manar.lashin@ejust.edu.eg
[d]Mechatronics and Robotics Eng. Dept., Egypt-Japan University of Science and Technology, E-JUST- Alexandria, Egypt mahmoud.magdi@ejust.edu.eg
[e]Mechatronics and Robotics Eng. Dept., Egypt-Japan University of Science and Technology, E-JUST- Alexandria, Egypt, on leave: Electrical Engineering Department, Faculty of Engineering, Assiut University, Egypt abdelfatah.mohamed@ejust.edu.eg

978-1-5090-6000-9/17/$31.00 ©2017 IEEE

II. SYSTEM DESCRIPTION

The proposed manipulator consists of two pantographs with a guiding mechanism for each, where they are virtually separated in Fig. 1, and the numbers indicate the coincidence points [6]. These pantographs are connecting together by means of two parallelograms with vertical axes joints. The manipulator has 3DOF decoupled translational motions in x-, y- and z-directions, where the parallelograms keep the orientation of the end-effector fixed. The actuators that control the translation motions along y- and z-directions are d_y and d_z respectively, and they are located at the extreme left point $O(x,y,z)$, where O is the origin of the fixed coordinate system $O-xyz$. The actuator of x-direction is d_x, where it is located at the right point of the other actuators as shown in Figs. 1 and 2. The axes x, y, and z coincide with the three actuation axes. Figures 3 and 4 show the cad model of the new compliant manipulator using circular notch hinge as illustrated in Fig. 5.

A. Kinematic Modeling

The mechanical system, shown in Fig. 2, contains three linear actuated joint variables as $q=[d_x,d_y,d_z]^T$ and the position vector of the end-effector is $p=[p_x,p_y,p_z]^T$, where the end-effector is link l_{10}. Assuming that $\overline{AC}=\overline{BC}=\overline{DF}=a$ and $\overline{CD}=\overline{BF}=\overline{FE}=b$. The following vector-loop closure equations can be determined using Figs. 2 as:

$$\vec{\mathbf{OE}}=\vec{\mathbf{OA}}+\vec{\mathbf{AD}}+\vec{\mathbf{DE}}, \tag{1}$$

$$\vec{\mathbf{OE}}=\vec{\mathbf{OB}}+\vec{\mathbf{BF}}+\vec{\mathbf{FE}}. \tag{2}$$

using equations 1 and 2, the relation between the input variables q and the position of the end-effector p is determined as [6]:

$$p=\begin{pmatrix} M_x & 0 & 0 \\ 0 & M_y & 0 \\ 0 & 0 & M_z \end{pmatrix} q. \tag{3}$$

where $M_x=1+\frac{b}{a}$ and $M_y=M_z=-\frac{b}{a}$ are the magnification factors in x-, y- and z-direction respectively. The relationship between the linear velocities of input joint variables $\dot{q}$ and those of the end-effector $\dot{p}$ can be defined as:

$$\dot{p}=\begin{pmatrix} M_x & 0 & 0 \\ 0 & M_y & 0 \\ 0 & 0 & M_z \end{pmatrix} \dot{q}. \tag{4}$$

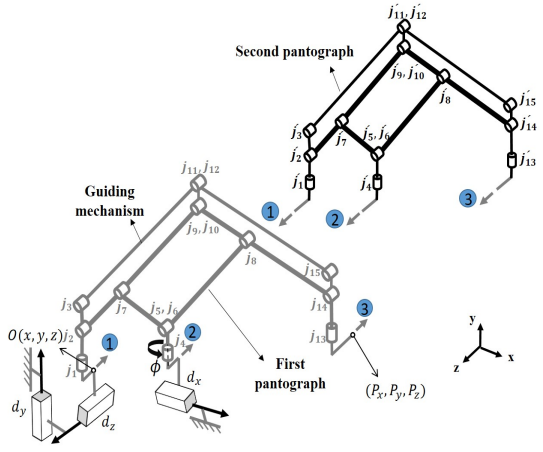

Fig. 1: Geometry of the 3D compliant manipulator

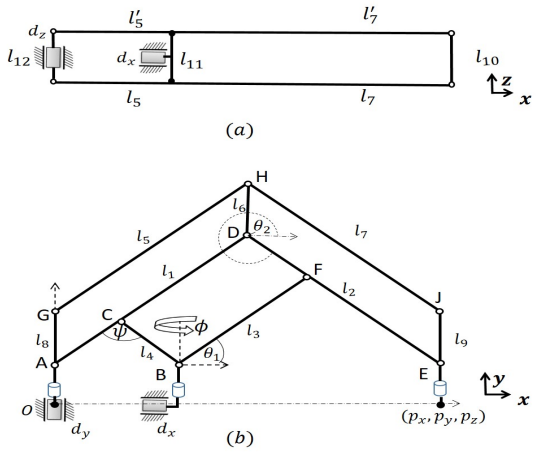

Fig. 2: Schematic drawing of the 3D compliant manipulator (a)Top view, (b)Front view

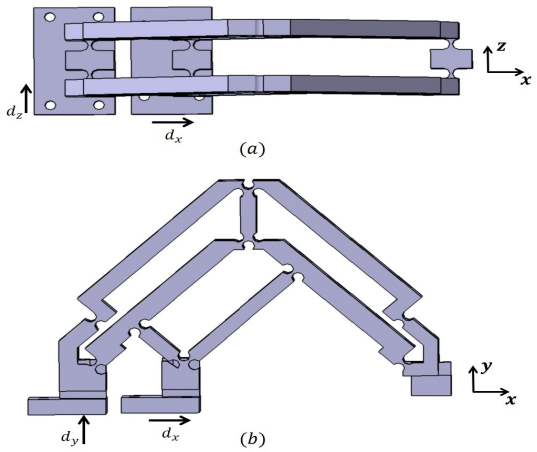

Fig. 3: The CAD model of the proposed manipulator (a)Top view, (b)Front view

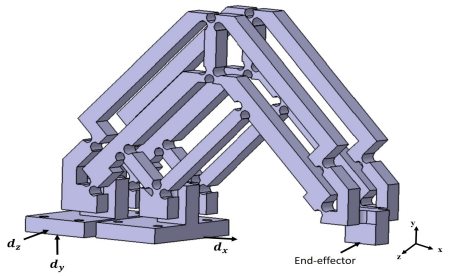

Fig. 4: The proposed compliant manipulator

B. Pseudo Rigid Body Model (PRBM)

The Pseudo-Rigid-Body Model (PRBM) concept is a systematic way that allows compliant mechanisms to be analyzed and modeled using a rigid-body mechanism, where each flexure hinge is replaced by a revolute joint and a torsional spring. PRBM was proposed by Howell in 1994 to predict the performance of the mechanism as a practical design method. The stiffness k of the torsional spring can be calculated for the circular notch joint by [5]:

$$k = \frac{2Ewt^{2.5}}{9\pi r^{0.5}}. \quad (5)$$

where E is the Young's modulus of the material, w, t and r are the width, thickness, and the radius of the joint respectively as described in Fig. 5.

III. PARAMETRIC DESIGN

The purpose of this section is to enhance the design of original manipulator using parametric design to enlarge the workspace and to eliminate the parasitic motions and geometric stiffening. Parametric design depends on the intuition and experience of the designer and this is done via investigating the influence of changing some design parameters which are many that affect the compliant manipulator performance. This section will only focus on four major parameters that have a considerable effect rather than the links' lengths a and b. Table I illustrates the physical constraints of the CPM, where only one parameter will be changed at a time. According to Table I and equation 3, the ideal magnification factors of input motion will be $M_x = 4$ and $M_y = M_z = -3$. It should be noted that t_z is the thickness of all joints having horizontal axes and t_y is the thickness of all joints having vertical axes.

TABLE I: Physical constraints

Physical constraint	**Value**
Pantograph lengths	$a = 15$ mm, $b = 45$ mm, and width=6 mm
Joint type	Circular notch joint
Joint Dimensions	$t_y = t_z = 0.8$ mm, $r = 2$ mm, and $w = 6$ mm
Actuators initial position	$d_{x0} = \frac{2a}{\sqrt{2}}$, $d_{y0} = 0$ mm, and $d_{z0} = 0$ mm
Material Properties	Structural steel Young's Modulus Yield strength Poisson's ratio $E = 200$ GPa $\sigma_y = 250$ MPa 0.3

A. Thickness of flexure joints (t_z)

This parameter is found to have a notable effect on both the magnification factors M_x, M_y and M_z and the parasitic motions. Figure 6 shows the effect of increasing joint thickness t_z on magnification factors during input motions in the three orthogonal directions, where M_{ij} is the magnification factor of undesired motion in i-direction during input motion along j-direction. Figure 6a illustrates that M_x is inversely proportional to the thickness t_z and it is changed considerably, while $|M_{yx}|$ is directly proportional to t_z and M_{zx} is unchanged during motion along x-direction. The increasing of t_z throughout the actuator movements along y-direction is depicted in Fig. 6b, where the magnification factor $|M_y|$ and $|M_{xy}|$ are slightly decreases and M_{zy} is unchanged. Figure 6c shows considerable effect of t_y during the motion along z-direction on the magnification factor $|M_z|$, while parasitic motions along x- and y-directions, M_{xz} and M_{yz}, are unchanged. Regarding the above results, the flexure joint thickness t_z should be very small to improve the magnification factor to be as near as ideal values and to reduce some of the parasitic motions as well. However, there are some limitations on designing a very small thickness of the flexure hinges depends on the fabrication process, material type, and required deflection.

B. Thickness of flexure joints (t_y)

Figure 7 shows the impact of joint thickness t_z on magnification factors during input motions along x-, y-, and z-directions. The magnification factor M_x is directly proportional to t_y according to Fig. 7a while it is noted that no notable effect occurs for M_{yx} and M_{zx}. Figure 7b shows a little effect of increasing t_y on the magnification factors $|M_y|$ and $|M_{xy}|$ while M_{zy} is not changed. Fig. 7c shows that $|M_z|$ is proportionally decreased with the increase of t_y while M_{xz} and M_{yz} are unchanged and kept in a very low limits approximately zero. It is clear that there is a trade off between M_z and both M_x and M_y and therefore t_y should be selected to compromise between values of magnification factors to get the highest performance.

C. Thickness of the main pantograph links (t_m)

Another parameter that has a considerable effect is the thickness (t_m) of links l_1 and l_2 in the main pantograph mechanism which is depicted in Fig. 2. Magnification factor M_x is increased and M_{yx} is decreased as a result of increasing the thickness t_m during motion along x-direction as shown in Fig. 8a. Figures 8b and 8c show that M_y and M_z are changed slightly while the rest of parasitic motions have constant values during translational displacement along y- and z-directions respectively.

D. Changing the initial actuator position

The previous parameters have a direct impact of the performance of the compliant mechanism. However, One of the drawbacks is the unequal rate of change for magnification

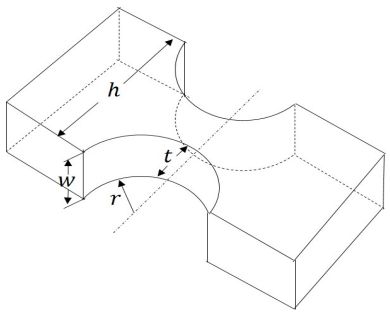

Fig. 5: Schematic of the flexure hinges

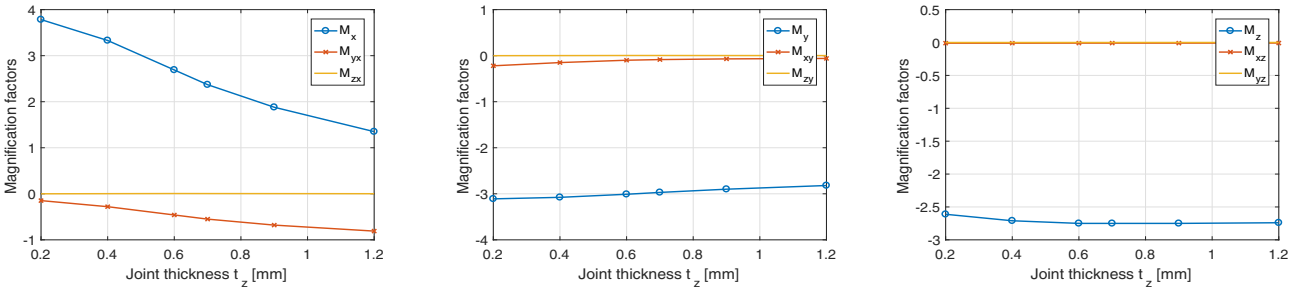

(a) Motion in **x**-axis (b) Motion in **y**-axis (c) Motion in **z**-axis

Fig. 6: Magnification factors versus joint thickness t_z

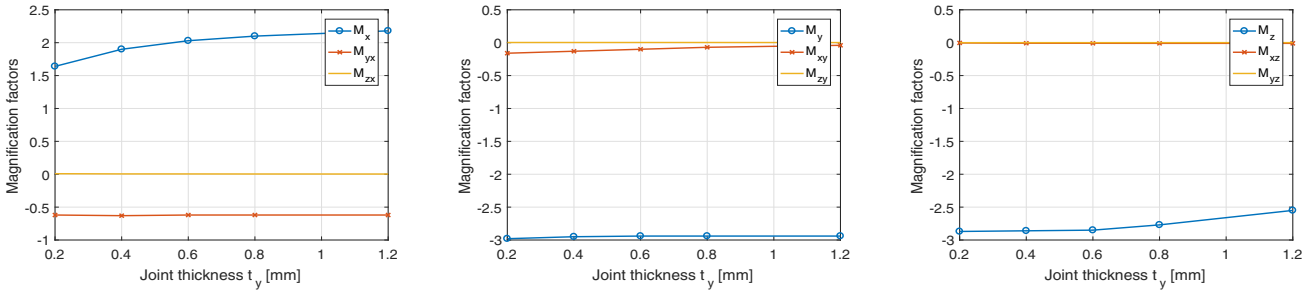

(a) Motion in **x**-axis (b) Motion in **y**-axis (c) Motion in **z**-axis

Fig. 7: Magnification factors versus joint thickness t_y

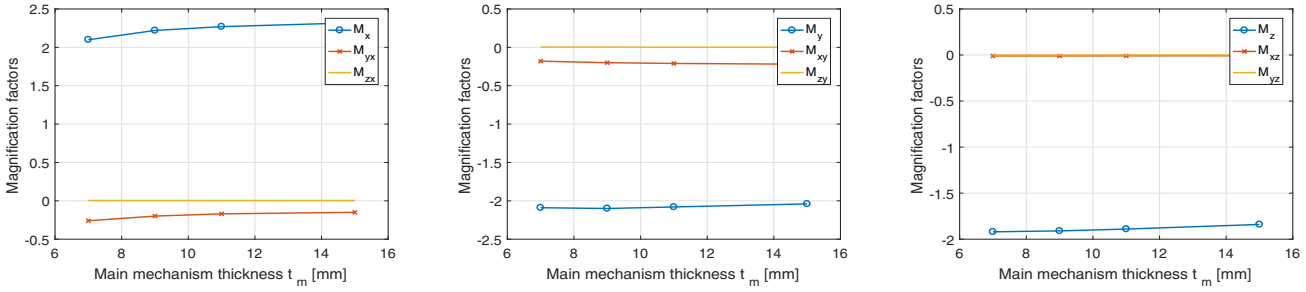

(a) Motion in **x**-axis (b) Motion in **y**-axis (c) Motion in **z**-axis

Fig. 8: Magnification factors versus links' thickness t_m

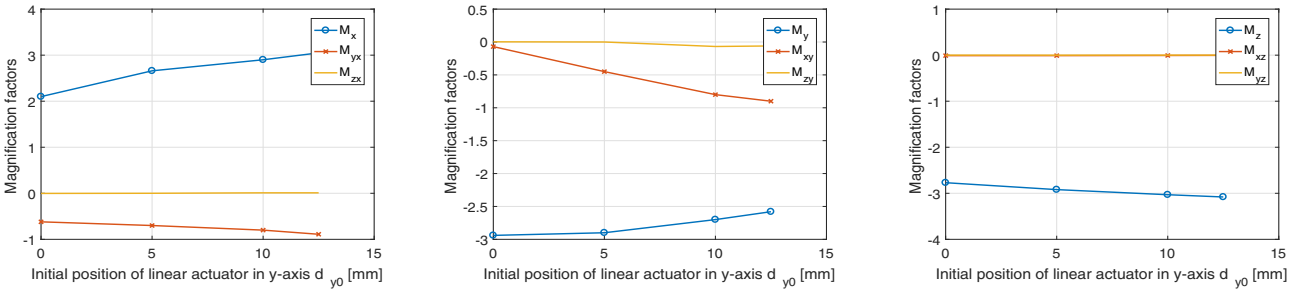

(a) Motion in **x**-axis (b) Motion in **y**-axis (c) Motion in **z**-axis

Fig. 9: Magnification factors versus initial actuator position d_{y_0}

factors especially for M_x and M_y. This could be compensated by changing the location of the actuator position d_x and d_y, at appropriate position along x- and y-axes respectively. Figure 2 shows that the initial location of the input actuator d_x along x-axis is $d_{x_0} = \frac{2a}{\sqrt{2}}$, while initial position of both actuators d_y and d_z are $d_{y_0} = 0\,\text{mm}$ and $d_{z_0} = 0\,\text{mm}$ respectively. There will be two objectives in this section; the first target is to reduce the rate of change for joint deflection during input motion which is directly proportional to the stress stiffening and the second target is to provide equivalent rate of change of the flexure joints for all input variables d_x, d_y and d_z. Referring to Fig. 10, the relation between the input motions d_x, d_y and d_z and deflection angle ψ is determined as:

$$d_x{}^2 + d_y{}^2 + d_z{}^2 = 2a(1 - \cos\psi), \tag{6}$$

hence,

$$\psi = \cos^{-1}(1 - \frac{d_x{}^2 + d_y{}^2 + d_z{}^2}{2a}). \tag{7}$$

The rate of change of the angle deflection ψ with respect to each input variables should be identical and equal to zero for the minimum deflection and stress stiffening and it can be written through the following equation:

$$\frac{\partial\psi}{\partial d_x} = \frac{\partial\psi}{\partial d_y} = \frac{\partial\psi}{\partial d_z} = 0. \tag{8}$$

The results for input variables d_x, d_y and d_z are found to be zero which should be the initial conditions for each. However, it will be a singular position at $d_x = 0\,\text{mm}$ consequently, d_{x_0} must take a value more than zero. As long as the rate of change of ψ is required to be equal with respect to input displacements especially for d_x and d_y, studying the influence of increasing d_{y_0} is carried out as shown in Fig. 9 at a constant value of length $\overline{AB} = \frac{2a}{\sqrt{2}}$. Figure 9a illustrates the increase of M_x and $|M_{yx}|$ during input motion d_x. The magnification factor of the parasitic motion $|M_{xy}|$ is increased, while $|M_y|$ is decreased when the manipulator is moving along y-axis as depicted in Fig. 9b. At input motion along z-axis, the magnification factor $|M_z|$ is increased although M_{xz} and M_{yz} are unchanged as shown in Fig. 9c. Based on the previous results, the parameters of the original manipulator could be changed to get significant improvements and also it could be done taking into account the design limitation and consideration for each parameter in fabrication process. The parameters of the proposed manipulator will be modified to be $t_z = 0.5\,\text{mm}$, $t_y = 0.85\,\text{mm}$, $t_m = 10\,\text{mm}$, $d_{x_0} = d_{y_0} = a$ and $d_{z_0} = 0\,\text{mm}$ as shown in Fig. 11 where the new magnification factors are shown in table II. The workspace volume is calculated for both the modified and the original manipulator as $0.0376\,\text{mm}^3$ and $0.0224\,\text{mm}^3$ respectively, where the actuators' stroke is $100\mu\text{m}\times100\mu\text{m}\times100\mu\text{m}$ for x-, y- and z-directions.

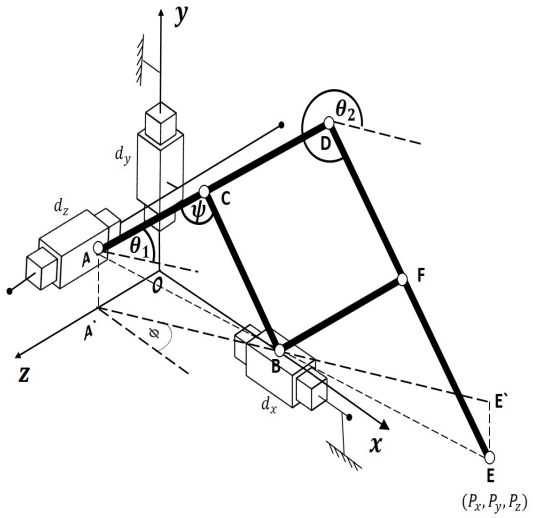

Fig. 10: Schematic drawing of the main pantograph mechanism

TABLE II: Magnification factors of the modified/original compliant manipulator

Input	$\frac{p_x}{d_{in}}$ **(new/old)**	$\frac{p_y}{d_{in}}$ **(new/old)**	$\frac{p_z}{d_{in}}$ **(new/old)**
d_x	M_x $4.02/2.67$	M_{yx} $0.13/-0.39$	M_{zx} $8.7\times10^{-5}/0.002$
d_y	M_{xy} $0.34/-0.11$	M_y $-3.09/-3.14$	M_{zy} $-8.1\times10^{-5}/0.002$
d_z	M_{xz} $0.01/0.01$	M_{yz} $0.001/0.004$	M_z $-3.03/-2.67$

IV. Frequency Analysis and Simulation

In this section, the modal analysis of the modified compliant manipulator is carried out in order to investigate the dynamic characteristics to be used in controller design. The prototype is built on CATIA® and tested using ANSYS® software. The first three mode shapes are translations along the three orthogonal axes as shown in Fig. 12, where $f_1 = 70.038\text{Hz}$, $f_2 = 93.863\text{Hz}$ and $f_3 = 126.11\text{Hz}$ are the first three natural frequencies respectively. The lowest natural frequency gives a useful insight into the dynamic performances of a mechanism. Consequently, the variation tendency of only the first natural frequency is obtained versus thickness of

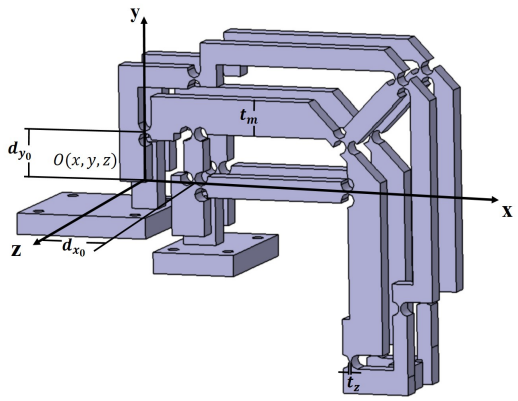

Fig. 11: The modified design of the proposed manipulator

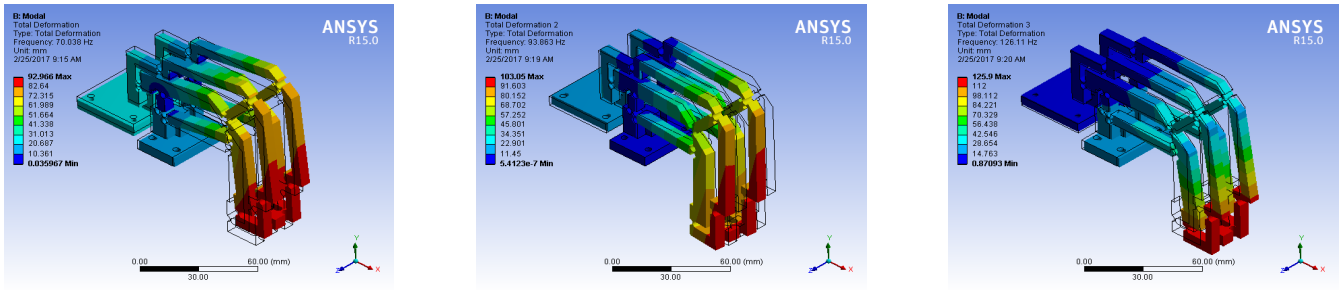

(a) First mode shape (b) Second mode shape (c) Third mode shape

Fig. 12: Mode shapes of the proposed manipulator

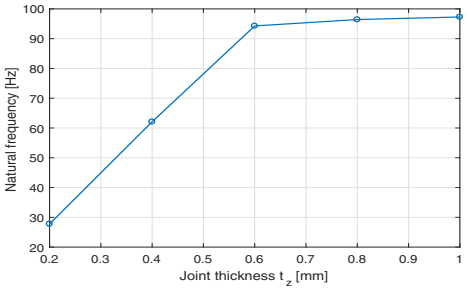

Fig. 13: Natural frequency versus joint thickness t_z

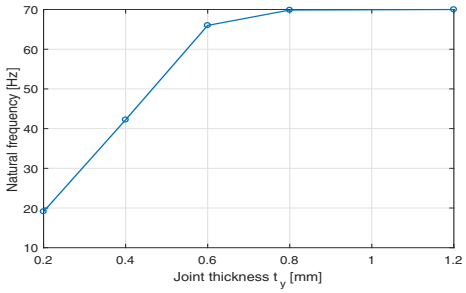

Fig. 14: Natural frequency versus joint thickness t_y

the flexure joints t_z and t_y. Figures 13 and 14 show that the frequency is directly proportional to the thickness t_z and t_y respectively. The frequency increases considerably at small values of thickness, whereas increases slightly when the thickness of both t_z and t_y are larger than 0.8mm.

V. CONCLUSIONS

New compliant parallel manipulator is designed based on parallelogram linkages using circular notch joint to give three decoupled translational motion with fixed orientation. The parametric design of the proposed manipulator is performed for major parameters that have a direct impact on the manipulator performance. Moreover, modal shapes and natural frequencies analysis are carried out using ANSYS software. The modified manipulator gives higher workspace, less joint stiffening, and parasitic motions. Furthermore, the results provide essential guidelines for controller design and geometry optimization.

ACKNOWLEDGMENT

The first author is supported by a scholarship from the Mission Department, Ministry of Higher Education of the Government of Egypt which is gratefully acknowledged.

REFERENCES

[1] Y. Li and Q. Xu, "Design and optimization of an xyz parallel micromanipulator with flexure hinges," *Journal of Intelligent and Robotic Systems*, vol. 55, no. 4-5, pp. 377–402, 2009.

[2] S. T. Smith, *Flexures: elements of elastic mechanisms*. CRC Press, 2000.

[3] Y. Tian, B. Shirinzadeh, D. Zhang, and Y. Zhong, "Three flexure hinges for compliant mechanism designs based on dimensionless graph analysis," *Precision Engineering*, vol. 34, no. 1, pp. 92–100, 2010.

[4] B. Zettl, W. Szyszkowski, and W. Zhang, "Accurate low dof modeling of a planar compliant mechanism with flexure hinges: the equivalent beam methodology," *Precision Engineering*, vol. 29, no. 2, pp. 237–245, 2005.

[5] B. H. Kang, J. T.-Y. Wen, N. Dagalakis, and J. J. Gorman, "Analysis and design of parallel mechanisms with flexure joints," *Robotics, IEEE Transactions on*, vol. 21, no. 6, pp. 1179–1185, 2005.

[6] A. T. Elgammal, M. Fanni, and A. M. Mohamed, "Design and analysis of a novel 3d decoupled manipulator based on compliant pantograph for micromanipulation," *Journal of Intelligent & Robotic Systems*, pp. 1–15, 2016.

[7] M. B. Parkinson, L. L. Howell, and J. J. Cox, "A parametric approach to the optimization-based design of compliant mechanisms," in *Proceedings of the 23rd Design Automation Conference, DETC97/DAC-3763*, 1997.

[8] Y. Li and Q. Xu, "Dynamics analysis of a modified 3-prc compliant parallel micromanipulator," in *Nanotechnology, 2007. IEEE-NANO 2007. 7th IEEE Conference on*, pp. 432–437, IEEE, 2007.

[9] X. Tang, H.-H. Pham, Q. Li, and I.-M. Chen, "Dynamic analysis of a 3-dof flexure parallel micromanipulator," in *Robotics, Automation and Mechatronics, 2004 IEEE Conference on*, vol. 1, pp. 95–100, IEEE, 2004.

[10] C. Kimball and L.-W. Tsai, "Modeling of flexural beams subjected to arbitrary end loads," *Journal of Mechanical Design*, vol. 124, no. 2, pp. 223–235, 2002.

[11] L. L. Howell, *Compliant mechanisms*. John Wiley & Sons, 2001.

[12] H. Shi, *Modeling and analysis of compliant mechanisms for designing nanopositioners*. PhD thesis, The Ohio State University, 2013.